

Article

Microfiber Coating for Flow Control over a Blunt Surface

Mitsugu Hasegawa  and Hirotaka Sakaue 

Department of Aerospace and Mechanical Engineering, University of Notre Dame, Notre Dame, IN 46556, USA; mhasegaw@nd.edu

* Correspondence: hsakaue@nd.edu; Tel.: +1-574-302-1747

Received: 23 August 2019; Accepted: 11 October 2019; Published: 14 October 2019



Abstract: A microfiber coating having a hair-like structure is investigated as a passive flow control device of a bluff body. The effect of microfiber length is experimentally studied to understand the impact of the coating on drag on a cylinder. A series of microfiber coatings with different lengths are fabricated using flocking technology and applied to various locations over the cylinder surface under the constant Reynolds number of 6.1×10^4 based on the diameter of the cylinder. It is found that the length and the location both play important roles in the drag reduction. Two types of drag reduction can be seen: (1) when the relative length of the microfiber, k/D , is less than 1.8%, and the coating is applied before flow separates over the cylinder; and (2) k/D is over 3.3%, and the coating is applied after the flow separation location on the cylinder. The maximum drag reduction for the former type is 59% compared to that from the cylinder without the microfiber coating. For the latter type, the maximum drag reduction is 27%.

Keywords: microfiber; electrostatic flocking; passive flow control; drag reduction

1. Introduction

Flow control over a bluff-body, especially drag reduction over a circular cylinder, is an engineering interest for broad applications in ground objects such as buildings, towers, bridges, or transportation systems like cars, trucks, rail, and airplanes [1–4]. Drag can be reduced actively or passively using a flow-control device. Active devices, such as plasma actuators, have significant effects on flow control which requires energy input for its operation [5,6]. However, application of the active devices is limited because of mechanical and electrical installation requirements. Passive devices, which do not require external energy, will be a practical option because of broader possible applications using engineered surfaces, materials, and coatings. Examples of passive devices are a trip rod [7–10], dimple [11,12], vortex generator [13,14], permeable surface [15–17], and riblets [18–20].

A microfiber coating having a hair-like structure has been paid attention for passive bluff-body drag reduction because its flexibility can produce a passive but adaptive influence on a flow, leading to drag and lift control. [21,22]. Hasegawa and Sakaue have investigated the application of microfiber coating by flocking technology to drag reduction on a cylinder [23]. In their study, it was found that drag was reduced due to delayed flow separation if the partial microfiber coating was applied before the point of flow separation. However, a drag reduction was not shown by the microfiber coating in the flow separation region. The microfiber length and the coating location were limited under their experiment. Further studies in microfiber length are necessary to reveal: (1) the correlation between microfiber length and coating location, and (2) the impact on drag by the microfiber coating in the separation region.

In the present study, a series of microfiber coatings of different lengths is experimentally studied to discuss the impact of the microfiber coating on drag. The location of each coating is scanned from

the leading edge to the trailing edge of a cylinder surface. A wake survey is used to evaluate the effects of the microfiber coating on the surface flow and obtain the drag coefficient.

2. Materials and Methods

A subsonic wind tunnel located at the Hessert Laboratory for Aerospace Research at the University of Notre Dame was used to conduct a wake survey of a cylinder with and without a microfiber coating. The test section has a 0.61 m square cross-section and a length of 1.83 m. The wind tunnel has an inlet contraction ratio of 20:1. A series of 12 turbulence management screens installed at the front of the inlet provided tunnel freestream turbulence levels of less than 0.1%.

A machined cylinder made of an engineering plastic was used. The cylinder had a 50 mm diameter, D , and a span length, L , of 610 mm; this gave an aspect ratio, L/D , of approximately 12. It was mounted horizontally in the test section. The solid blockage ratio was 8%. The freestream velocity, U_∞ , was 20 m/s for all test cases. The Reynolds number based on the cylinder diameter, D , was 6.1×10^4 .

A microfiber coating was applied over the cylinder surface. Various combinations of coating location and microfiber length were chosen. Figure 1a schematically describes a configuration of the coating over the cylinder. The microfiber length is denoted as k . The coating location, θ , is an angular position described by the angle measured from the front edge of the coating toward the leading edge of the cylinder. The streamwise width of the microfiber coating was fixed at $0.3D$ (15 mm) for all test cases. Figure 1b,c show representative images of the microfiber coating with $k = 0.91$ mm captured with a microscope (AM4115ZT, Dunwell Tech. Inc, Torrance, CA, USA). The fabricated microfiber coating showed variation in the azimuthal angle, while the microfiber coating in Figure 1a illustrates an ideal condition with perfect alignment.

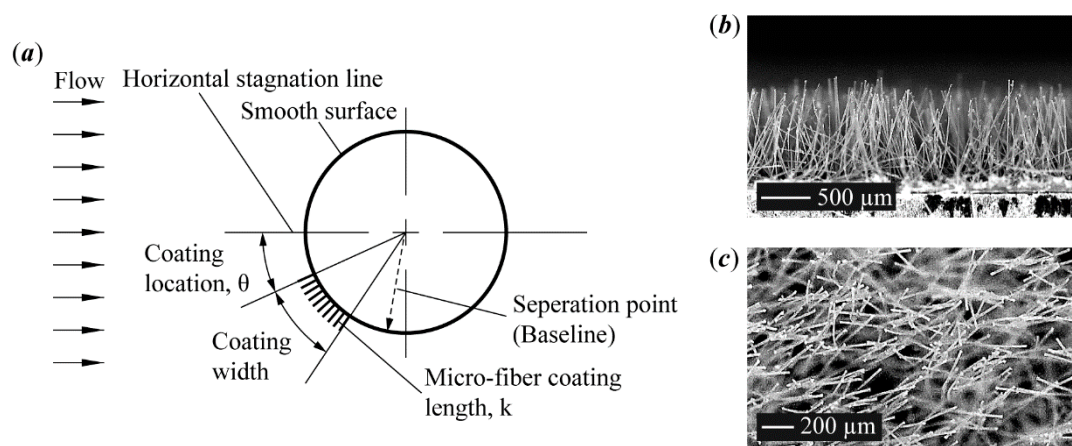


Figure 1. A schematic of a microfiber coating over the cylinder model: (a) Coating configuration on the cylinder model; (b) a microscope image of fabricated microfiber coating, side view ($k = 0.91$ mm); (c) a microscope image of fabricated microfiber coating, top view ($k = 0.91$ mm).

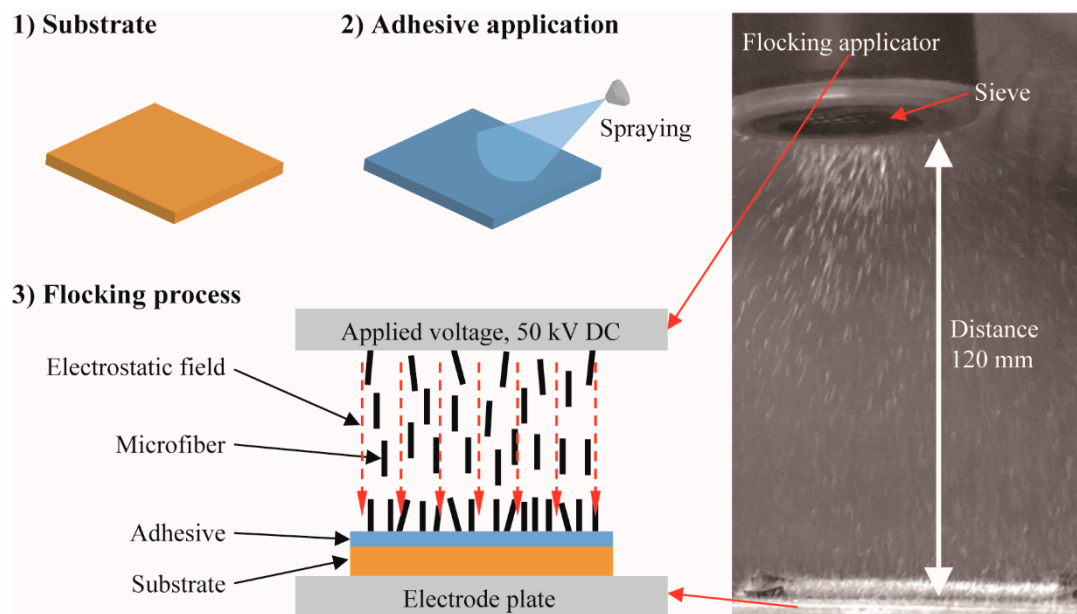
Coating parameters are summarized in Table 1. The averaged microfiber length was measured on images of samples captured with a microscope (AM4115ZT, Dunwell Tech. Inc, Torrance, CA, USA) which was calibrated with a stage micrometer. The relative length of the microfibers, defined as k/D , ranges from 1.1% to 9.0%. Under the present Reynolds number, a smooth cylinder, which was the cylinder without the microfiber coating used as a baseline, experienced a subcritical regime flow with distinctive flow regions: an attached flow region with a laminar boundary layer, and a separated-flow region consisting of free shear layers and the wake region [24]. Based on these flow features, the effect of the microfiber coating on the attached-flow and the separated-flow regions was studied by varying the coating location.

Table 1. Microfiber coating parameters.

Microfiber Length, k [mm]	Relative Length, k/D [%]	Coating Location, θ [°]
0.54 ± 0.05	1.1	10 to 120
0.91 ± 0.03	1.8	10 to 120
1.52 ± 0.09	3.0	10 to 140
1.67 ± 0.16	3.3	10 to 140
2.53 ± 0.04	5.1	10 to 140
4.52 ± 0.13	9.0	10 to 140

2.1. Fabrication of Microfiber Coating

The microfiber coating was fabricated using an electrostatic flocking method [23,25,26]. Figure 2 schematically describes the process of the fabrication method of the microfiber coating. Under an electrostatic field, microfibers are implanted in an adhesive layer. Nylon 6/6, Poly (hexamethylene adipamide, Campbell Coutts Ltd., Eastleigh, UK) was chosen for the microfiber because of its elasticity and resiliency, which are preferred for a self-adaptive structure, and its excellence in abrasion resistance for durability. Epoxy adhesive was applied on a film (Simair, UK) with a thickness of 50 μm .

**Figure 2.** Fabrication process of microfiber coating.

2.2. Wake Survey

Figure 3 shows a schematic of the wake survey setup. Dynamic pressure, q_{wake} , at 25 data points was scanned over a range that was $\pm 3D$ in the vertical axis from the horizontal centerline of the cylinder. The interval of scanning points was 12.7 mm. A step motor traverse system with a step motor driver (PDO3540, Applied Motion Products, Watsonville, CA, USA) was used to vertically traverse the wake flow using a pitot-static tube. Wake measurements were performed at $4D$ downstream from the trailing edge of the cylinder. For the freestream measurement, a freestream dynamic pressure, q_{∞} , was also measured at $4D$ upstream from the cylinder. To read dynamic pressures, a pressure transducer (DATUM 2000, Setra Systems, Boxborough, MA, USA) with a full-scale range of 0 to 127 mm of water column was used. It has an accuracy of $\pm 0.14\%$ of its full-scale reading. The output signal from the transducer was read by a DAQ system (DT9836, Data Translation, Marlborough, MA, USA) with 16-bit analog/digital channels. Each pressure measurement was sampled at 1 kHz for 10 s. Post-processed averaged data was used for the drag estimation.

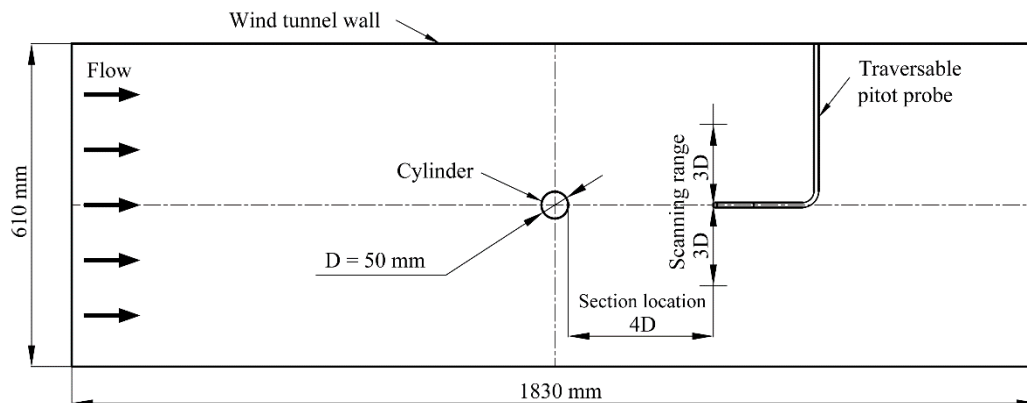


Figure 3. A schematic of the wake survey setup in the test section.

2.3. Drag Estimation

The drag coefficient was estimated using a two-dimensional integral momentum balance method [27]. The following expression for the drag coefficient per unit span of a cylinder, c_d , is given as:

$$c_d = \frac{2}{D} \int_{y=-3D}^{y=+3D} \left(\sqrt{\frac{q_{\text{wake}}}{q_{\infty}}} - \frac{q_{\text{wake}}}{q_{\infty}} \right) dy, \quad (1)$$

where q_{∞} and q_{wake} are the dynamic pressures in the freestream and downstream of the cylinder, respectively. Then, a normalized drag coefficient, which is normalized by the drag coefficient of the baseline, $c_{d\text{-baseline}}$, was obtained:

$$c_{d\text{-norm}} = \frac{c_d}{c_{d\text{-baseline}}}, \quad (2)$$

where the normalized drag coefficient, $c_{d\text{-norm}}$ below unity shows a drag decrease, while a drag increase is shown above unity.

3. Results

3.1. Drag Estimation

Figure 4 shows the summary of the drag estimates obtained from the cylinder with microfiber coatings. The normalized drag coefficient, $c_{d\text{-norm}}$, described in Equation (2) was shown with various relative microfiber lengths and coating locations.

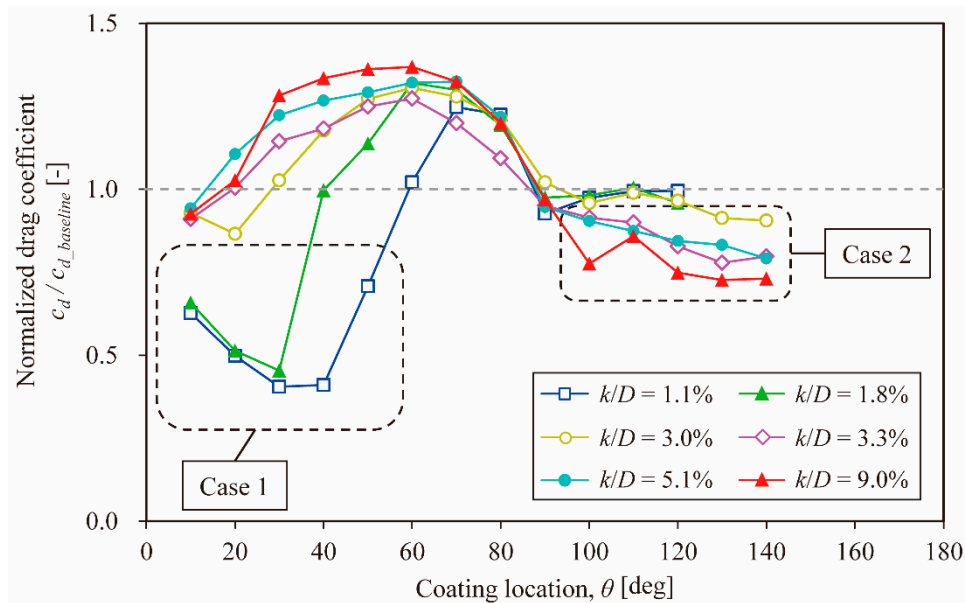


Figure 4. Comparison of drag varying with relative microfiber length and coating location.

The following remarks were found from Figure 4: (1) Excellent drag reduction was achieved for microfiber coatings with $k/D \leq 1.8\%$ at $10^\circ \leq \theta \leq 30^\circ$ (see Case 1). It includes a maximum 59% drag reduction by the microfiber coating with $k/D = 1.1\%$ at $\theta = 30^\circ$. (2) Moderate drag reduction was achieved with $k/D \geq 3.3\%$ at $100^\circ \leq \theta \leq 140^\circ$ (see Case 2). It includes a maximum 27% drag reduction by the microfiber coating where $k/D = 9.0\%$ at $\theta = 130^\circ$. (3) Maximum drag increase was shown at $60^\circ \leq \theta \leq 70^\circ$ regardless of the relative length of the microfibers. The key from these facts is that both the relative length of the microfibers and the coating location impacted drag. As a summary: (1) Drag reduction (see Case 1) can be performed if we apply a microfiber coating before the point of flow separation. Here, the point of flow separation occurred at $\theta = 70^\circ$ to 80° for the baseline measurement. (2) Drag (see Case 2) can be reduced if we apply a microfiber coating after the point of flow separation. The critical length of microfiber was $k/D < 3.0\%$ for Case 1 and $k/D \geq 3.0\%$ for Case 2 under the present Reynolds number.

The drag reduction mechanism for Case 1 would be the same function as a boundary layer trip [23]. The coating location for Case 1 corresponds to a laminar boundary layer under the present flow condition. The presence of the microfiber coating can add disturbances into the flow. Such disturbance will trigger a boundary layer transition from laminar to turbulent boundary layer and cause high momentum fluids in the free stream to be injected into near-wall flow, which leads to strong near-wall momentum. This results in a flow separation delay which can contribute to significant reduction of drag on the cylinder shown where $k/D = 1.1\%$ and $k/D = 1.8\%$ at $\theta = 30^\circ$. However, incomplete boundary layer transition or slight separation delay could be caused if the coating location is not suitable; the rate of drag reduction of $k/D = 1.1\%$ and $k/D = 1.8\%$ changed depending on the coating location at between $\theta = 10^\circ$ and 50° . The relative length of the microfibers is also an essential factor to cause the boundary layer to trip as is the case with the concept of roughness critical height [28,29]. However, the microfiber coating could cause an early flow separation that can be seen as a drag increase when the relative fiber length is longer than $k/D = 3.0\%$. Figure 5 shows a schematic of a profile of a circular cylinder with a microfiber coating at $\theta = 30^\circ$. As k/D increases, the microfiber coating can relatively protrude outside boundary layer, δ/D , which is on the order of $O(1/Re^{0.5}) \sim 0.01$, and changes the overall profile of the cylinder significantly like a step shown in Figure 5b [24]. Although the microfiber coating is permeable, flow, including external flow over the cylinder with the microfiber coating, could be significantly affected by the step-change which resulted in flow separation as k/D increased.

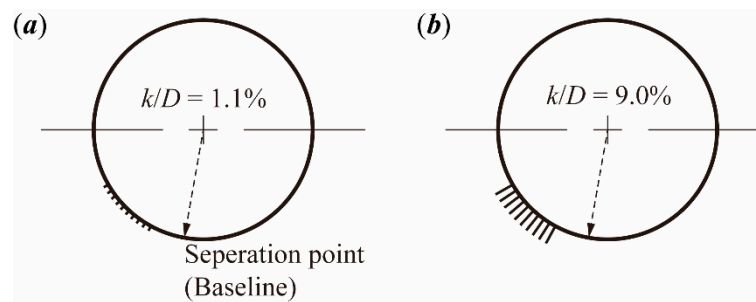


Figure 5. A schematic of overall profile of a circular cylinder with microfiber coating at a coating location of $\theta = 30^\circ$: (a) $k/D = 1.1\%$; (b) $k/D = 9.0\%$.

The microfiber coating applied after the point of flow separation performed a drag reduction (see Case 2). However, it is still questionable that the mechanism is an enhancement of flow attachment which we expected the effect of the microfiber coating to be in the separation region [23]. The mitigation of shear layer and vortex circulation at the rear side of the cylinder would be one of the potential mechanisms. Interaction of the microfiber coating with a shear layer from the cylinder surface could lead to a drag reduction. The coating location in Case 2 corresponded to a flow separation region where a backflow and a shear layer were present [24]. Under the baseline flow, a periodic swirling by the backflow and the shear layer will be present at the rear side of a cylinder after the separation point. The lengthy microfiber coating at the rear side could interact with a shear layer or both shear layer and backflow depending on the microfiber length. It could mitigate a shear flow and vortex circulation due to the shedding vortices at the rear side of the cylinder. Figure 6 shows a schematic of a profile of a circular cylinder with microfiber coating at $\theta = 120^\circ$. In the view of topology, a longer fiber as shown in Figure 6b significantly changes a cylinder profile which has a larger effect on flow, while shorter fibers shown in Figure 6a seems to have little impact. As k/D increases, it can be expected that the microfiber coating interacts with the backflow in the wake with larger effect which leads to further drag reduction. The presence of such relatively long microfiber coatings at the leeward side of the cylinder also seems to be similar to a tab mounted on the trailing edges or a splitter plate on a bluff body which tend to attenuate Karman vortex shedding, resulting in drag reduction [4].

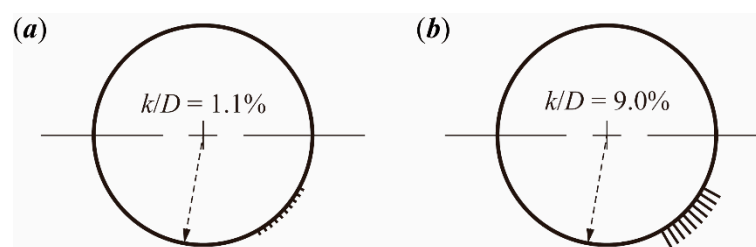


Figure 6. A schematic of overall profile of a circular cylinder with microfiber coating at a coating location of $\theta = 120^\circ$: (a) $k/D = 1.1\%$; (b) $k/D = 9.0\%$.

A potential reason for maximizing drag between $60^\circ \leq \theta \leq 70^\circ$ would be due to the induced flow separation [10,29]. In this region, the baseline flow almost started to separate due to the flow acceleration under the adverse pressure gradient over a cylinder surface. The presence of the coating could enhance or trigger early flow separation which leads to a drag penalty. This severe drag penalty can be seen if the coating when the relative length of $k/D > 3.0\%$ is applied before the point of flow separation.

3.2. Wake Survey

Figure 7 shows a comparison of mean velocity profiles in the wake regions obtained from the baseline and from the microfiber coatings with three different lengths. The relative fiber lengths from

$k/D = 1.1\%$, 1.8% , and 9.0% showed the effect of microfiber coatings on the distinctive drag impact discussed in the previous section. The mean velocity profile, $u(y)$, and vertical position of wake scan, y , were normalized by the freestream velocity, U_∞ , and the cylinder diameter, D , respectively. The asymmetric velocity profiles came from an asymmetry of the coating location to the horizontal axis. As described in the experimental section, the coating was only applied in the negative y region in the present study. For the coating location at $\theta = 30^\circ$ shown in Figure 7a, we can see a major velocity change at $y/D < 0$ compared to the baseline due to the asymmetrical coating application. The velocity deficit for the microfiber length, $k/D = 1.1\%$ and 1.8% was significantly reduced. It corresponded to a narrowed wake zone due to the flow separation delay by the microfiber coating as we discussed about the Case 1 drag reduction in the previous section. On the other hand, the longest microfiber length, $k/D = 9.0\%$, showed an increase in velocity deficit which leads to drag increase. For the coating location at $\theta = 60^\circ$ shown in Figure 7b, the coatings with $k/D = 1.1\%$ and 9.0% showed an obvious increase in velocity deficit which was shown as a drag penalty in Figure 4. The amount of the velocity deficit obtained from the coating with $k/D = 9.0\%$ was greater than that at $\theta = 30^\circ$. The velocity deficit in the wake profile ranged widely, which could be due to an early flow separation. The coating with $k/D = 1.1\%$ at $\theta = 60^\circ$ was almost the same profile as the baseline. Both coating location and coating length influence the flow. For the coating location at $\theta = 120^\circ$ shown in Figure 7c, the coating with $k/D = 9.0\%$ showed a moderate reduction of the velocity deficit which corresponds to the Case 2 drag reduction discussed in the previous section. The shorter microfibers with $k/D = 1.1\%$ and 1.8% were almost overlapped with the baseline result and it can be found that the shorter fiber did not function reasonably for drag reduction.

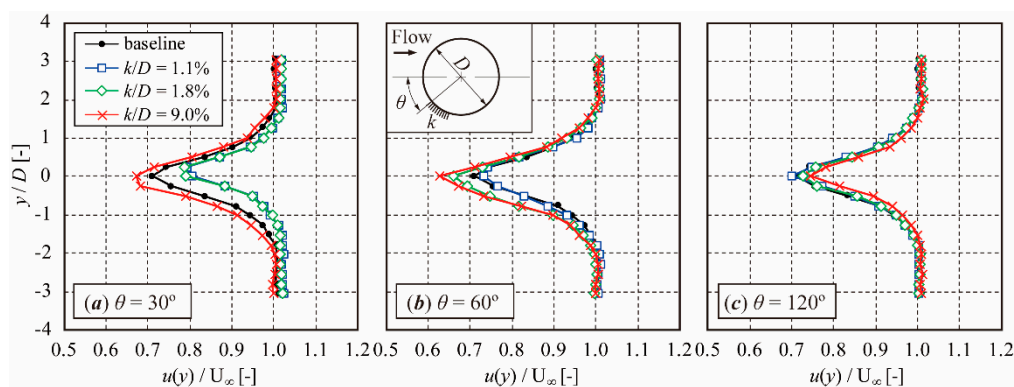


Figure 7. Comparison of mean velocity profiles in the wake for baseline and microfiber with relative length of $k/D = 1.1\%$, 1.8% , and 9.0% : (a) $\theta = 30^\circ$; (b) $\theta = 60^\circ$; and (c) $\theta = 120^\circ$.

4. Conclusions

A microfiber coating having a hair-like structure was introduced as a passive flow control device for bluff-body drag reduction. The effects of the microfiber coating on drag were experimentally evaluated by a wake survey and the two-dimensional integral momentum balance method. The effect on drag by correlation between microfiber length and the coating location were considered. To reveal the effects of the microfiber coating, the Reynolds number was fixed at 6.1×10^4 based on the cylinder diameter. It was found that both the length of the microfiber and the location were important parameters to reduce drag. Drag reduction was seen from a shorter microfiber with $k/D \leq 1.8\%$. The coating should be located within $10^\circ \leq \theta \leq 30^\circ$, where θ is an angle from the leading edge to the trailing edge of the cylinder chord. A maximum drag reduction of 59% was obtained compared to the drag without the microfiber coating. Drag reduction was seen from a longer microfiber with $k/D \geq 3.3\%$ at the coating location within $100^\circ \leq \theta \leq 140^\circ$ where the coating is located in the separation region; a maximum drag reduction of 27% was obtained. Since density and orientation of microfiber coating would be another influencer on flow, further studies in controllability of the density and orientation are considered.

Author Contributions: Conceptualization, H.S. and M.H.; methodology, H.S. and M.H.; validation, M.H.; formal analysis, H.S. and M.H.; investigation, M.H.; writing—original draft preparation, M.H.; writing—review and editing, H.S.; supervision, H.S.; project administration, H.S.; funding acquisition, H.S.

Funding: This research was funded by the Operational Energy Capability Improvement Fund (OECIF) from the Office of the Assistant Secretary of Defense for Operational Energy Plans and Programs, ASD (OEPP), and the Air Force Research Laboratory (AFRL) through Ohio Aerospace Institute (OAI), grant number OAI-ESMCND-1600012.

Conflicts of Interest: The authors declare no conflict of interest.

References

1. Bishop, R.E.D.; Hassan, A.Y. The lift and drag forces on a circular cylinder in a flowing fluid. *Proc. R. Soc. Lond. Ser. A Math. Phys. Sci.* **1964**, *277*, 32–50.
2. Prasad, A.; Williamson, C.H.K. A method for the reduction of bluff body drag. *J. Wind Eng. Ind. Aerodyn.* **1997**, *69–71*, 155–167. [[CrossRef](#)]
3. Matsumoto, M. Vortex shedding of bluff bodies: A review. *J. Fluids Struct.* **1999**, *13*, 791–811. [[CrossRef](#)]
4. Choi, H.; Jeon, W.-P.; Kim, J. Control of Flow Over a Bluff Body. *Annu. Rev. Fluid Mech.* **2008**, *40*, 113–139. [[CrossRef](#)]
5. Thomas, F.O.; Kozlov, A.; Corke, T.C. Plasma Actuators for Cylinder Flow Control and Noise Reduction. *AIAA J.* **2008**, *46*, 1921–1931. [[CrossRef](#)]
6. Kozlov, A.V.; Thomas, F.O. Bluff-Body Flow Control via Two Types of Dielectric Barrier Discharge Plasma Actuation. *AIAA J.* **2011**, *49*, 1919–1931. [[CrossRef](#)]
7. Wieselsberger, C. Der luftwiderstand von kugeln. *Z. Flugtech. Motorluftschiffahrt* **1914**, *5*, 140–145.
8. Fage, A. The effects of turbulence and surface roughness on the drag of a circular cylinder. *Rep. Memo.* **1929**, *1283*, 1–8.
9. James, D.F.; Truong, Q.-S. Wind load on cylinder with spanwise protrusion. *J. Eng. Mech. Div.* **1972**, *98*, 1573–1589.
10. Nebres, J.; Batill, S. Flow about a circular cylinder with a single large-scale surface perturbation. *Exp. Fluids* **1993**, *15*, 369–379. [[CrossRef](#)]
11. Bearman, P.W.; Harvey, J.K. Control of circular cylinder flow by the use of dimples. *AIAA J.* **1993**, *31*, 1753–1756. [[CrossRef](#)]
12. Choi, J.; Jeon, W.-P.; Choi, H. Mechanism of drag reduction by dimples on a sphere. *Phys. Fluids* **2006**, *18*, 041702. [[CrossRef](#)]
13. Lin, J.C.; Robinson, S.K.; McGhee, R.J.; Valarezo, W.O. Separation control on high-lift airfoils via micro-vortex generators. *J. Aircr.* **1994**, *31*, 1317–1323. [[CrossRef](#)]
14. Lin, J.C. Review of research on low-profile vortex generators to control boundary-layer separation. *Prog. Aerosp. Sci.* **2002**, *38*, 389–420. [[CrossRef](#)]
15. Bruneau, C.-H.; Mortazavi, I. Control of Vortex Shedding Around a Pipe Section Using a Porous Sheath. *Int. J. Offshore Polar Eng.* **2006**, *16*, 7.
16. Bhattacharyya, S.; Singh, A.K. Reduction in drag and vortex shedding frequency through porous sheath around a circular cylinder. *Int. J. Numer. Methods Fluids* **2011**, *65*, 683–698. [[CrossRef](#)]
17. Klausmann, K.; Ruck, B. Drag reduction of circular cylinders by porous coating on the leeward side. *J. Fluid Mech.* **2017**, *813*, 382–411. [[CrossRef](#)]
18. Walsh, M.J. Riblets as a Viscous Drag Reduction Technique. *AIAA J.* **1983**, *21*, 485–486. [[CrossRef](#)]
19. Bechert, D.; Reif, W. On the Drag Reduction of the Shark Skin. In *Proceedings of the 23rd Aerospace Sciences Meeting*; American Institute of Aeronautics and Astronautics: Reston, VA, USA, 1985.
20. Lee, S.-J.; Lim, H.-C.; Han, M.; Lee, S.S. Flow control of circular cylinder with a V-grooved micro-riblet film. *Fluid Dyn. Res.* **2005**, *37*, 246–266. [[CrossRef](#)]
21. Favier, J.; Dauphinais, A.; Basso, D.; Bottaro, A. Passive separation control using a self-adaptive hairy coating. *J. Fluid Mech.* **2009**, *627*, 451–483. [[CrossRef](#)]
22. Brucker, C. Interaction of flexible surface hairs with near-wall turbulence. *J. Phys. Condens. Matter* **2011**, *23*, 18. [[CrossRef](#)] [[PubMed](#)]
23. Hasegawa, M.; Sakaue, H. Microfiber Coating for Drag Reduction by Flocking Technology. *Coatings* **2018**, *8*, 464. [[CrossRef](#)]

24. Sumer, B.M.; Fredsoe, J. *Hydrodynamics Around Cylindrical Structures*; Advanced Series on Ocean Engineering; World Scientific: Singapore, 2006; Volume 26, ISBN 978-981-270-039-1.
25. Bolgen, S.W. Flocking Technology. *J. Coat. Fabr.* **1991**, *21*, 123–131. [[CrossRef](#)]
26. Woodruff, F.A. Developments in Coating and Electrostatic Flocking. *J. Coat. Fabr.* **1993**, *22*, 290–297. [[CrossRef](#)]
27. Barlow, J.B.; Rae, W.H.; Pope, A.; Pope, A. *Low-Speed Wind Tunnel Testing*; Wiley: Hoboken, NJ, USA, 1999; ISBN 9780471557746.
28. Braslow, A.L.; Knox, E.C. *Simplified Method for Determination of Critical Height of Distributed Roughness Particles for Boundary-layer Transition at Mach Numbers from 0 to 5*; National Advisory Committee for Aeronautics: Washington, WA, USA, 1958.
29. Igarshi, T. Characteristics of the Flow around Two Circular Cylinders Arranged in Tandem: 1st Report. *Bull. JSME* **1981**, *24*, 323–331. [[CrossRef](#)]



© 2019 by the authors. Licensee MDPI, Basel, Switzerland. This article is an open access article distributed under the terms and conditions of the Creative Commons Attribution (CC BY) license (<http://creativecommons.org/licenses/by/4.0/>).